Flow and Particle Deposition using an Integrated CFD Model of the Respiratory System

Aleck H. ALEXOPOULOS,[2] Paraskevi KARAKOSTA[2] and Costas KIPARISSIDES*[1,2]

* Corresponding author: Tel.: +(30) 2310996212; Fax: +(30) 2310 498160;
Email: cypress@cperi.certh.gr
1: Department of Chemical Engineering, Aristotle University of Thessaloniki, P.O. Box 472, Thessaloniki, Greece.
2: Chemical Process Engineering Research Institute, CERTH, Thermi, Greece:

Abstract In the present study a theoretical investigation on flow, particle motion, and deposition in the respiratory system is reported. An integrated computational model of the respiratory system is developed comprised of nine sequential computational blocks corresponding to the nasal cavity, the pharyngo-trachea, and a series of branches of the pulmonary system. Airflow during steady-state inhalation inside the human respiratory system was determined using computational fluid dynamics (CFD) for inlet velocities, v_{in} = 1-20 m/s, corresponding to inhalation flow rates of 9 to 180 L/min, and particle deposition was examined in detail for particle sizes, D=1-20μm. Local deposition efficiencies as well as spatial distribution of deposited particles were found to be strongly dependent on the particle size and volumetric flow rate.

Keywords: Respiratory, pulmonary, CFD, Particles, CFD, deposition, nasal,

1. Introduction

The transfer and deposition of particles in the respiratory system is of major interest to the scientific and medical community in terms of the development of targeted drug delivery formulations but also due to the increasing concerns over the potential toxicity of natural and engineered micro- and nanoparticles (Illum, 2006; Sharma et al. 2009; Azarmi et al., 2008; Weinhold and Mlynski, 2004, Oberdörster et al., 2005). Experimental and theoretical work have focused on different regions of the respiratory system, e.g., oropharyngeal, nasal, pulmonary, and alveolar regions, where many aspects of particle penetration and deposition have been investigated (Wang et al., 2009; Heenan et al., 2003; van Ertbruggen et al., 2005; Doorly et al., 2008). However, several issues remain to be elucidated including the deposition of non-spherical particles and fibres, particle dispersion and aggregation, the effects of particle size and shape and finally the fate of deposited particles and their impact on biological systems.

The current "virtual physiological human" (VPH) European initiative aims to develop a methodological and computational framework to enable investigations of the human body as an integrated system (Fenner et al., 2008; Kohl and Noble, 2009). The main goal is to achieve a systematic approach of describing the human body that avoids the pitfalls of subdividing biological systems in any particular way. The VPH initiative encompasses a diverse range of research disciplines and holds immense promise for the future in terms of improving our understanding of the physiome, training, surgery planning, diagnostics and therapeutics. Although significant progress has been made towards the development of a virtual respiratory system many challenges lie ahead including the development of accurate models to describe soft-tissue deformation (e.g., of stromal tissue and pleural walls), generation and motion of mucous layers in healthy and diseased states, particle penetration through the mucosa and alveoli, as well as cellular and sub-cellular models of pulmonary epithelial cells (Burrowes et al., 2008; Sloot and Hoekstra, 2009; Sun et al., 2007).

Accurate 3D geometrical descriptions of the

pulmonary tract geometry as well as the corresponding pulmonary circulatory system are necessary to determine interactions with parenchymal tissue and oxygen transfer to the pulmonary vascular systems and thus evaluate respiratory diseases such as hepatopulmonary syndrome (Tawhai et al., 2004; Chakraborty et al., 2007). Consequently, it has become increasingly apparent that multi-scale, multi-physics models are necessary to describe the respiratory system from cellular and sub-cellular levels up to the tissue and bulk levels (Burrowes et al., 2008) and to improve our understanding on particle motion, deposition, and penetration in the respiratory system.

Previous computational models of the respiratory system have employed multiple or single computational blocks. Yu et al. (1998) and Martonen et al. (2002) first described single-block models extending from the nasal cavity down to the first bronchial branch of the pulmonary system. Computational models describing larger portions of the pulmonary system were developed with the computational blocks corresponding to individual pulmonary branches (Zhang et al., 2009) or groups of pulmonary branches (Nowak et al., 2003).

In this work a multi-block computational model is proposed in which the respiratory system is assumed to consist of nine sequential computational blocks (Figure 1). The computational blocks are connected by the entry/exit boundary conditions, e.g., the outflow conditions of a computational block are used as inflow conditions of the subsequent block. Steady-state airflow in the respiratory system during inhalation is determined by performing CFD simulations in each computational block. Particle deposition is determined by Eulerian-fluid/Lagrangian-particle simulations. In the following sections a description of the CFD approach is provided (2) and computational results for the nasal cavity (section 3.1), the pharyngotrachea (section 3.2), and the pulmonary system (section 3.3) are presented.

2. Multi-block Model of the Respiratory System

The respiratory pathway studied in this work consists of the nasal cavity, the nasopharynx, and the pulmonary tract. The nasal cavity is formed by two nasal air paths converging posteriorly to the nasopharynx, which is directed downwards to the pharynx and the trachea. The two nasal air paths are highly curved and convoluted in shape providing a total surface area of about 150 cm^2 (Proctor and Anderson, 1982; Cole, 2000). The nasal walls are covered by a mucous layer which moves to the posterior of the nasal cavity clearing deposited particles. The flow and deposition of particles in the nasal cavity has been investigated by several groups (Wang et al., 2009; Liu et al., 2007; Wen et al., 2008; Subramaniam et al., 2008; Hörschler et al., 2003; Inthavong et al., 2008; Shi et al., 2007).

The pharyngotracheal route has been studied not only to determine particle depositions but also to determine the function of the larynx (Tao and Jiang, 2008). There are two main constrictions to airflow: one at the top adjacent to the oral cavity and the second near the larynx (Fig. 1).

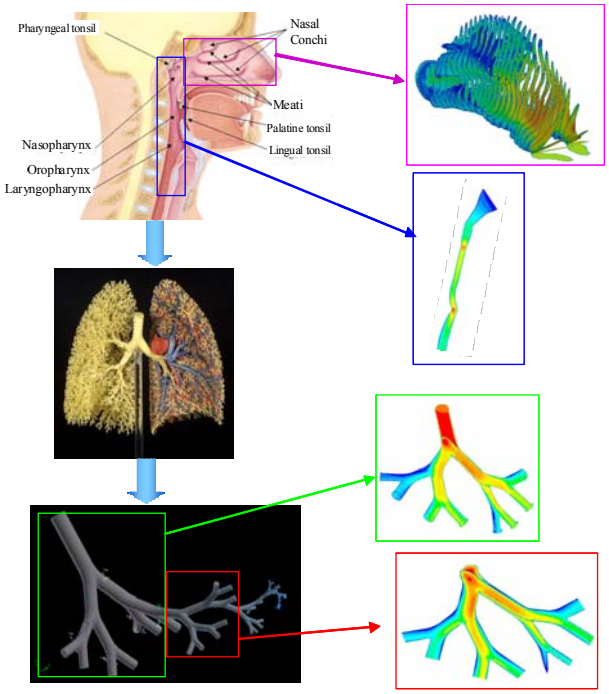

Fig. 1 *Block Computational Structure of the Respiratory System.*

The pulmonary system consists of a multitude of nonsymmetrical branches of progressively smaller diameter. There are a total of 23-24 branch generations leading to about 10^8 simple

branches in the entire pulmonary system (Finlay, 2004). This multi-branch geometry presents serious limitations on the number of branch generations that can be fully simulated by CFD (van Ertbruggen et al., 2005; Zhang et al., 2009; Longest and Vinchurkar, 2007) although simplified descriptions of flow can be employed to describe the lower branches (Tawhai et al., 2009). However, if a single airflow path-line (i.e., sequence of pulmonary branches) in the pulmonary system is considered, and other parallel paths are ignored, a successive simulation approach can be followed from the bronchi down to the alveolar sacs (Nowak et al., 2003).

The multi-block computational model of this work consists of nine computational blocks. The first block corresponds to the inflow cavity, e.g., the nasal or the oral cavity, the second block connects the inflow cavity to the lower trachea just above the first pulmonary bifurcation. The computational blocks that follow represent the branching structure of the pulmonary tract. Each computational block of the pulmonary system consists of three generations of symmetrical branches. Half the 2^{nd} and 3^{rd} generation branches of each computational block are rotated 90 degrees with respect to the plane of the first branch leading to an overall nonplanar configuration (see Figure 1 inset).

3. Results and Discussion

Numerical simulations of steady inhalation in the respiratory system as well as particle depositions were performed using the CFD commercial software FLUENT (v6.3). The numerical simulations were performed with double precision, implicit time stepping, and second order gradients. The convergence criteria for all the residuals were set to 10^{-4}. The flow field calculations were conducted on a PC type Dell Workstation (8 core Xeon 5300) with 20G memory. The CPU time for simulating the flow field was 1-50 hours per processor depending on the computational mesh, type of flow, and the Reynolds number.

Results are presented for the velocity magnitude and the local particle deposition efficiency in the nasal cavity, the pharyngotrachea, and the initial blocks of the pulmonary system. Particle deposition is determined by an Eulerian/Lagrangian tracking scheme based on the steady-state solutions for flow obtained from the CFD simulation results. Particles were released uniformly from the inlet surface and both uniform and Rosin-Rammler size distributions are employed to determine overall and local particle deposition profiles.

3.1. Results for the Nasal Cavity

The nasal cavity geometry was reconstructed based on a series of medical images and is similar to the geometry described in Shi et al. (2007). A number of different computational grids consisting of tetrahedral cells were generated varying from about 2.7 10^5 to 2.2 10^6 in number with a skewness of less than 0.8 (Kammona et al., 2010). Because of the nature of the flow in the nasal cavity the transitional SST k-ω model was employed as a good compromise between laminar and fully-developed turbulent flow.

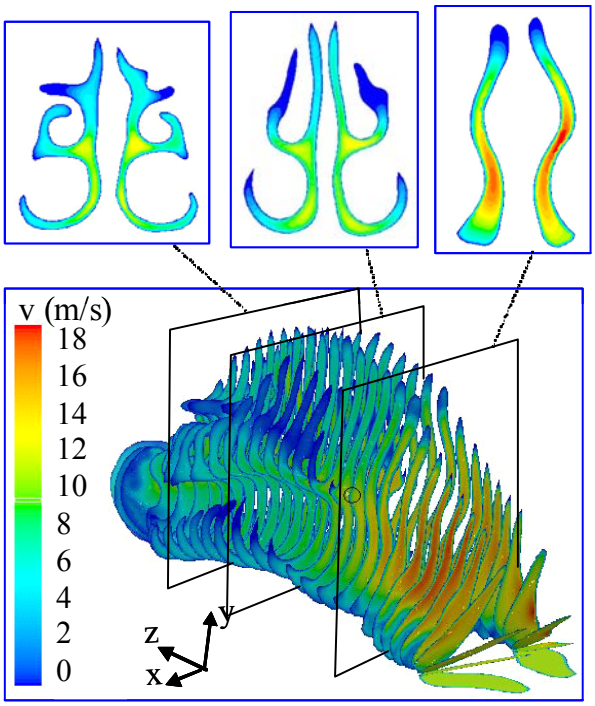

Fig. 2. *Velocity magnitude in the nasal cavity. Coronal sections. Inlet velocity* v_{in} *= 10m/s*

The velocity magnitude at several coronal slices was obtained for different inlet velocities. As can be seen in Figure 2 the incoming airflow accelerates and reaches

maximum velocity in the nasal valve region after which it decelerates and is directed towards the intersection of the nasal meati where the cross-sectional area is largest and the resistance to flow the lowest. Although nasal cavity geometries vary significantly between individuals the observed flow patterns that have been observed in the literature possess similar characteristics (Subramaniam et al., 1998; Inthavong, 2008). Nasal airflow permits sufficient conditioning of inflowing air (in terms of humidity and temperature) and adequate mixing up to the sensitive olfactory region, situated in the upper region of the nasal cavity, while at the same time providing a significant capture rate of large (i.e., >5μm) particles.

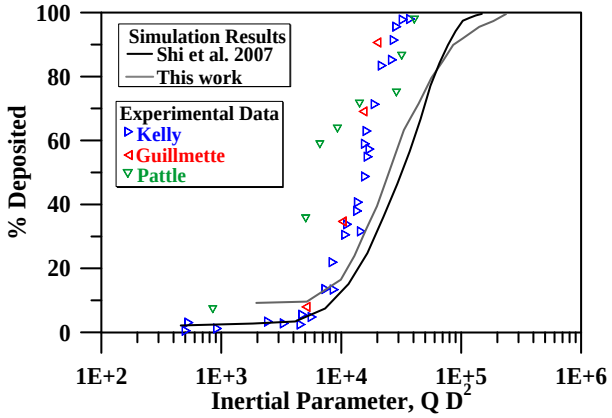

Fig. 3. *Deposition Efficiency in the Nasal Cavity. Comparison to literature experimental data and simulation results.*

For micron sized particles inertial effects dominate over Brownian motion and larger particles are deposited more efficiently. For inertia-dominated cases, particle deposition efficiency is typically described in terms of the impaction parameter, QD^2, where Q is the volumetric flow rate and D the particle diameter. In Figure 3 the percent deposition efficiency predicted by two different simulations (Shi et al., 2007; Kammona et al., 2010) is compared to available experimental data (from different nasal geometries). The best predictions by two-equation models of turbulence (i.e., k-ω) slightly under-predict the experimental data. This could be due to enhanced deposition due to surface charge or surface roughness effects (Shi et al. 2007).

An important aspect of nasal and pulmonary systems is the cilia-driven motion of the mucosal layer which constitutes a mechanism for clearance of deposited particles. Due to mucosal motion the deposited particles have a finite residence time which depends on the particle-mucosa interactions but also on the particle deposition position in the respiratory tract, e.g., particles depositing deeper in the pulmonary system require more time to be removed by the mucosa. Consequently, spatial or axial particle deposition profiles are important and these can be determined from simulation results.

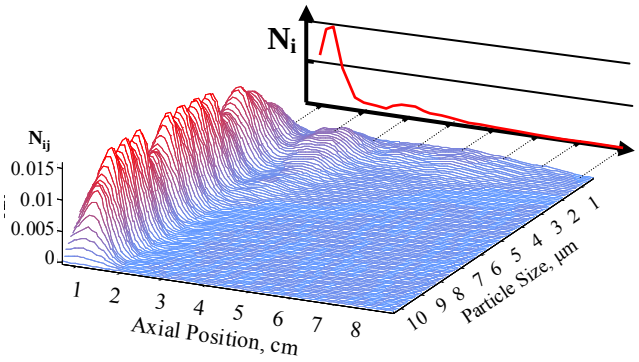

Fig. 4. *Univariate and bivariate particle deposition profiles in the nasal cavity. Injected particles: Rosin-Ramler distribution D_{ave}=10μm. Inlet velocity v_{in}=2m/s.*

In Figure 4 univariate and size-dependent bivariate axial deposition profiles in the nasal cavity are shown for an inlet velocity of v_{in} = 2m/s. It is observed that the larger particles are mostly deposited in the anterior region of the nasal cavity and in smaller amounts in the medial regions. Similar graphs with smaller sized particles indicate decreased deposition numbers but a more uniform spatial deposition pattern (Kammona et al., 2010).

It should be noted that the axial particle deposition pattern can be determined from the CFD simulation results and, if the velocity of mucosal motion is known, can be expressed in terms of residence time of the deposited particles in the nasal cavity. Particles depositing in the posterior and anterior regions of the nasal cavity have short and long residence times, respectively. In a recent publication this residence time information was connected to a simple drug release model

to determine the amount of antibody encapsulated nanoparticles that penetrate to the mucosal layer (Kammona et al., 2010).

3.2. Results for the PharyngoTrachea

The computational geometry was obtained by extending the nasopharyngeal region of the posterior nasal cavity downwards towards the pharynx and trachea. The geometric description of the pharyngotrachea by Heenan et al. (2003) was employed without the oral cavity and by extension to the nasopharnyx. The pharyngotracheal geometry was then simplified and described as a curved conduit of changing cross-sectional area and shape leading to a smoothed computational grid consisting of 88,000 tetrahedral cells.

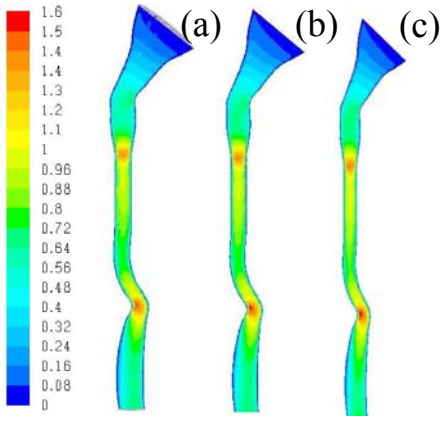

Fig. 5. *Relative velocity magnitude in the pharyngotrachea pathway (v/v_{in}). (a) v_{in} = 2 m/s, (b) 5 m/s, (c) 10 m/s.*

In Figure 5 the velocity magnitude of airflow in the pharyngotracheal region is displayed for three different inhalation velocities, i.e., v_{in} = 2, 5, and 10m/s. It is observed that the airflow accelerates in the converging nasopharyngeal region adjacent to the nasal cavity. Peak velocities are observed at positions corresponding to narrow cross-sectional positions observed just above the oral cavity and in the laryngeal region. It should be noted that the flow profiles are qualitatively similar in this smoothed geometry and only minor differences can be observed in Figure 5.

Particle motion and deposition in the pharyngotrachea was determined by Eulerian/Lagrangian simulations based on CFD solutions for steady inhalation. The number of particles injected at the inlet surface of the nasorpharynx is equal to the number of particles exiting the nasal cavity. These particles enter the nasopharynx following continuous trajectories from the nasal cavity or are redistributed evenly over the nasopharynx entry surface. It was found that larger particles deposit much more efficiently than smaller ones and most of the particle deposition occurs in the regions were flow is constricted. In fact, in more realistic non-smoothed geometries the deposition is expected to be even more localized in the constriction regions.

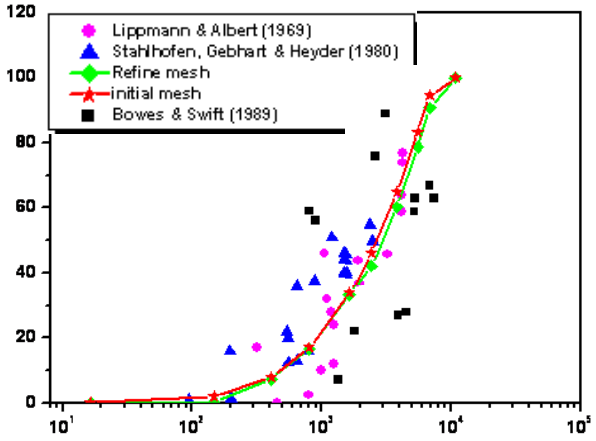

Fig. 6 Comparison of simulation results to literature data for inertial particles (D>1μm).

Particle depositions in the pharyngotrachea were determined for a number of different particle sizes (i.e., 1-20μm) and inhalation flow rates. Figure 6 compares the local deposition efficiencies in the pharyngotrachea with some literature data. The local deposition efficiency, ε_i, is based on the number of particles entering the i^{th} computational block. The total deposition efficiency, E_i, is thus equal to: $E_i = \varepsilon_i (1-\varepsilon_{i-1}) \ldots (1-\varepsilon_1)$. It is observed that the simulation results are in good agreement to the literature data (Bowes and Swift, 1989; Lippmann and Albert, 1969; Stahlhofen et al., 1980) for inertial particles despite the simplifications in the geometry of the nasopharynx.

3.3. Results for the Pulmonary System

The pulmonary tract is represented by a sequence of seven multi-branched computational blocks each of which is

discretized into 260,000 tetrahedral cells. The overall branch dimensions follow the geometrical model of Horsfield et al. (1971). Therefore, although the first pulmonary computational block, is different to the actual unsymmetrical branched structure of the pulmonary system, the following blocks are quite similar to the actual pulmonary structure.

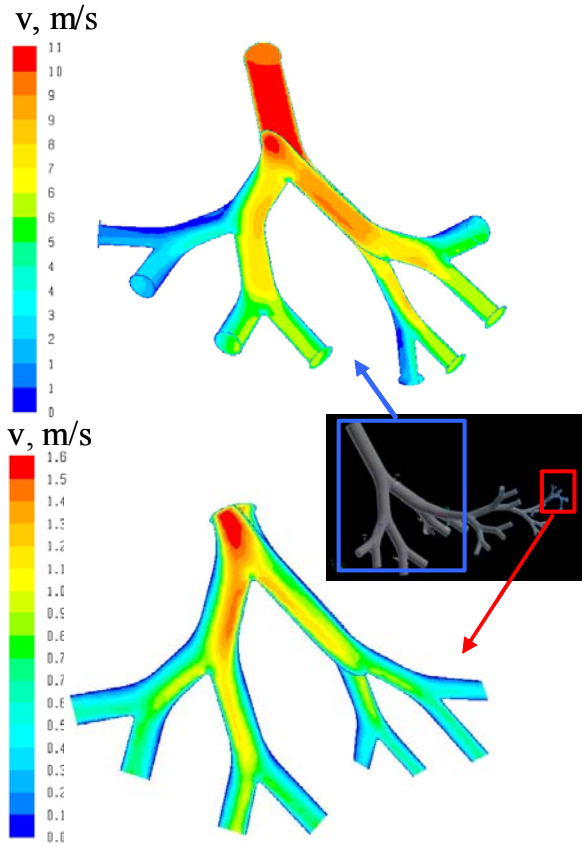

Fig. 7 *Velocity magnitudes in the pulmonary tract or different computational blocks (a) Block one, (b) Block four.* v_{in} *= 2.7m/s.*

Different computational geometries and grids were constructed by altering the sequence of blocks, e.g., by selecting different outflow branches to create the computational block sequence. It should be noted that in order to minimize the sensitivity of block selection on the final solution the results of this paper correspond to block selections that were based on the outflows which were closer to the mean outflow flow rate.

CFD simulations were performed for steady-state inhalation assuming k-ω turbulence model for the first blocks and switching to laminar flow after block 3 or 4 depending on the inhalation flow rate.

In Figure 7 the velocity magnitudes are shown for blocks one and four for an inhalation velocity of v_{in} = 2.7 m/s. It is clear that the velocity magnitude decreases with each block sequence as the airflow is split into an increasing number of airstreams. Furthermore, qualitative airflow differences are observed. The fundamental reason for these differences is that the distance between two successive branches is insufficient to achieve fully developed flow. Consequently, different branch sequences, e.g., different computational block sequences, will generate different results in terms of local airflow and particle deposition.

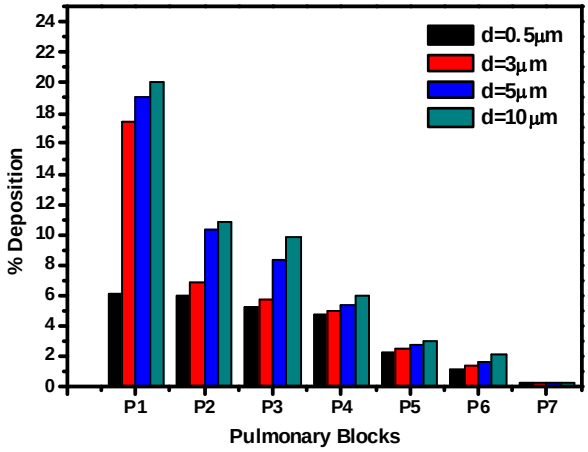

Fig. 8 *Local particle deposition efficiencies in the pulmonary tract.* v_{in} *= 5 m/s.*

In Figure 8 the local deposition efficiencies in the computational blocks of the pulmonary tract for an inhalation velocity of v_{in} = 5m/s are displayed. It is clear that, the deposition efficiencies decrease with each successive block due to a decrease in the airflow rate. On the other hand, for each block the local deposition efficiency increases with particle size from 0.5 to 10μm. The results for blocks six and seven were found to be sensitive to block selection and were difficult to obtain due to the decreased number of particles reaching the deepest branches of the pulmonary system. These results for local particle deposition efficiencies are in qualitative agreement to the results reported in the literature, e.g., Nowak et al. (2003).

Figure 9 displays the calculated local

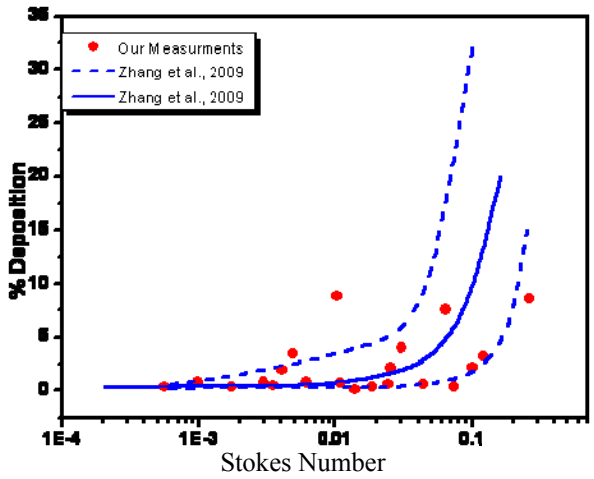

Fig. 9 *Local deposition efficiencies in the pulmonary tract.*

deposition efficiencies for different blocks of the pulmonary system in terms of the particle Stokes number for an inhalation velocity v_{in} = 10m/s and different particle sizes compared to the reported results of Zhang et al. (2009). It is observed that the results of this work are more dispersed than those of Zhang et al. (2009). One reason for this is the use of a nonplanar computational block as opposed to Zhang et al. (2009) and Nowak et al. (2003) who used symmetrical and planar blocks.

4. Conclusions

The proposed integrated multi-scale multi-block computational approach, despite its many simplifications, can describe airflow and particle deposition profiles in the respiratory system. The computed particle deposition profiles in terms of local deposition efficiency appear to be in qualitative agreement with experimental and computational data. Deposition of large (i.e., >1μm) particles are dominated by inertia and local deposition efficiencies scale with QD^2 in the nasal and pharyngotracheal regions. In the pulmonary region the analysis of particle deposition is made difficult by the asymmetrical particle pathlines, even with symmetrical pulmonary geometries, which makes the choice of results sensitive to the computational block sequence. Despite these limitations the proposed multi-block computational approach shows promise in describing full deposition profiles throughout the respiratory system and can prove to be a very useful tool in simulating drug delivery by inhalation. To this end the multi-block model needs to be extended to include alveolar sacs and individual alveoli and the first pulmonary block needs to be replaced with a more realistic representation of the nonsymmetrical branch physiology. Finally, the numerical simulations need to be extended to a full breathing cycle (i.e., inhalation and exhalation) to best represent the transitional nature of respiratory flow and its effect on particle deposition in the branched structure of the pulmonary system.

References

Azarmi, S., W.H. Roa, R. Lobenberg, Targeted delivery of nanoparticles for the treatment of lung diseases. Advanced Drug Delivery Reviews 60 (2008) 863-875.

Bowes, S.M. and D.L. Swift, 1989. Deposition of inhaled particles in the oral airway during oronasal breathing. Aerosol Sci. Technol. 11, 157-167.

Burrowes, K.S., A.J. Swan, N.J. Warren, and M.H. Tawhai, Towards a virtual lung: multi-scale, multi-physics modeling of the pulmonary system, Phil. Trans. R. Soc. A 366 (2008) 3247-3263.

Chakraborty, S., V. Balakotaiah, and A. Bidani, 2007. Multiscale model for pulmonary oxygen uptake and its application to quantify hypoxemia in hepatopulmonary syndrome. J. of Theoretical Biology 244, 190-207.

Cole, P., 2000. Biophysics of nasal airflow: a review. Am. J. Rhinology 14, 245-249.

Doorly, D.J., D.J. Taylor, A.M. Gambaruto, R.C. Schroter, and N. Tolley, Nasal architecture: form and flow. Phil. Trans. R. Soc. A 366 (2008) 3225-3246.

Fenner, J.W., B. Brook, G. Clapworthy, P.V. Coveney, V. Feipel, H. Gregersen, D.R. Hose, P. Kohl, P. Lawford, K.M. McCormack, D. Pinney, S.R. Thomas, S. Van Sint Jan, S. Waters and M. Viceconti, 2008. The EuroPhysiome, STEP and a roadmap for the virtual physiological human. Phil. Trans. R. Soc. A *366:1878*, 2979-2999.

Finlay, W.H., 2004. Lung Deposition Simulation, in Hickey, A.J. (ed.) Pharmaceutical Inhalation Aerosol Technology, Marcel Dekker, NY.

Heenan, A.F., Matida, E., Pollard, A., Finlay, W.H., 2003. Experimental measurements and computational modeling of the flow in an idealized human oropharynx, Experiments in Fluids 35, 70-84.

Kammona, O., A.H. Alexopoulos, P. Karakosta, K. Kotti, V. Karageorgiou and C. Kiparissides. Nanocarrier Aided Nasal Vaccination: An

Experimental and Computational Approach, Ind. Eng. Chem. Res. (2010) in press.

Horsfield, K., G., Dart, D.E. Olson, G.F. Filley, and G. Cumming Models of the Human Bronchial Tree, J. of Applied Physiology, 31 (1971) 207-217.

Hörschler, I., M. Meinke, and W. Schröder, Numerical simulation of the flow field in a model of the nasal cavity. Computers and Fluids 32 (2003) 39–45.

Inthavong, K., J. Wen, Z.F. Tian, and J.W. Tu, Numerical study of fibre deposition in a human nasal cavity. Aerosol Science 39 (2008) 253–265.

Kohl, P. and D. Noble, 2009. Systems biology and the virtual physiological human. Molecular Systems Biology 5:292, 1-6.

Illum, L. Nanoparticulate systems for nasal delivery of drugs: a real improvement over simple systems?, J. Pharm. Sci. 96 (2006) 473-483.

Lippmann, M. and R.E. Albert, 1969. The effect of particle size on the regional deposition of inhaled aerosols in the human respiratory tract. Am. Ind. Hyg. Assoc. J. 30, 257-263.

Liu, Y., Matida, E.A., Gu, J., Johnson, M.R., 2007. Numerical simulation of aerosol deposition in a 3-D human nasal cavity using RANS, RANS/EIM, and LES, Aerosol Sci. 38, 683-700.

Longest, P. and Vinchurkar S., 2007. Validating CFD predictions of respiratory aerosol deposition: Effects of upstream transition and turbulence, J. of Biomechanics 40(20), 305-316.

Martonen, T.B., Zhang, Z., Yue, G., Musante, C.J., 2002. 3-D particle transport within the human upper respiratory tract, Aerosol Science 33, 1095-1110.

Nowak, N., Kakade, P.P., Annapragada, A.V., 2003. Computational Fluid Dynamics Simulation of Airflow and Aerosol Deposition in Human Lungs, Annals of Biomed. Engineering 31, 374-390.

Oberdörster, G., E. Oberdörster, and J. Oberdörster, Nanotoxicology: An Emerging Discipline Evolving from Studies of Ultrafine Particles. Environmental Health Perspectives 113 (2005) 823-839.

Proctor, D.F. and I. Andersen, The nose – Upper airway physiology and the atmospheric environment, Elsevier Biomedical Press, Amsterdam, 1982.

Sharma, S., T.K.S. Mukkur, H.A.E. Benson, and Y. Chen, 2009. Pharmaceutical aspects of intranasal delivery of vaccines using particulate systems. J. Pharm. Sci. 98, 812-843.

Shi, H.W., C. Kleinstreuer, and Z. Zhang, 2007. Modeling of inertial particle transport and deposition in human nasal cavities with wall roughness. Aerosol Science 38, 398-419.

Sloot, P.M.A. and A.G. Hoekstra, Multi-scale modeling in computational biomedicine, Briefings in Bioinformatics 11 (2009) 142-152.

Stahlhofen, W., J. Gebhart, and J. Heyder, 1980. Experimental determination of the regional deposition of aerosolparticles in the human respiratory tract. Am. Ind. Hyg. Assoc. J., 41, 385-398.

Subramaniam, R.P., R.B. Richardson, K.T. Morgan, and J.S. Kimbell, 1998. Computational fluid dynamics simulations of inspiratory airflow in the human nose and nasopharynx. Inhalation Toxicology 10, 91-120.

Sun, X., C. Yu, Y. Wang, and Y. Lin, 2007. Numerical simulation of soft palate movement and airflow in human upper airway by fluid-structure interaction method. Acta Mech. Sin. 23, 359-367.

Tao, C. and J. Jiang, 2008. A self-oscillating biophysical computer model of the elongated vocal fold. Computers in Biology and Medicine *38,* 1211-1217.

Tawhai, M.H., P. Hunter, J. Tschirren, J. Reinhardt, G. McLennan, and E.A. Hoffman, 2004. CT-based geometry analysis and finite element models of the human and ovine bronchial tree. J. Appl. Physiol. 97, 2310-2321.

Tawhai, M.H., E.A. Hoffman, and C.-L. Lin, The lung physiome: merging imaging based measures with predictive computational models, Syst. Biol. Med., 1 (2009) 61–72.

van Ertbruggen, C., Hirsch, C., Paiva, M. 2005. Anatomically based three-dimensional model of airways to simulate flow and particle transport using computational fluid dynamics, J. Appl. Physiol. 98, 970-980.

Wang, S.M., K. Inthavong, J. Wen, J.Y.Tu, and C.L.Xue, Comparison of micron- and nanoparticle deposition patterns in a realistic human nasal cavity. Respiratory Physiology & Neurobiology 166 (2009) 142-151.

Weinhold, I. and G. Mlynski 2004. Numerical Simulation of Airflow in the Human Nose. Eur. Arch. Otorhinolaryngol. 261, 452-455.

Wen, J., Inthavong, K., Tu, J., Wang, S., 2008. Numerical simulations for detailed airflow dynamics in a human nasal cavity, Respiratory Physiology & Neurobiology.

Yu, G., Zhang, Z., Lessmann, R., 1998. Fluid Flow and Particle Diffusion in the Human Upper Respiratory System, Aerosol Science and Technology 28(2), 146-158.

Zhang, Z., Kleinstreuer, C., Kim, C.S., 2009. Comparison of analytical and CFD models with regard to micron particle deposition in a human 16-generation tracheobronchial airway model, Aerosol Science 40, 16-28.